Universal mean moment rate profiles of earthquake ruptures

Amit P. Mehta* and Karin A. Dahmen†

Department of Physics, University of Illinois at Urbana-Champaign, 1110 West Green Street, Urbana, Illinois 61801-3080, USA

Yehuda Ben-Zion‡

Department of Earth Sciences, University of Southern California, Los Angeles, California 90089-0740, USA
(Received 29 August 2005; published 5 May 2006)

Earthquake phenomenology exhibits a number of power law distributions including the Gutenberg-Richter frequency-size statistics and the Omori law for aftershock decay rates. In search for a basic model that renders correct predictions on long spatiotemporal scales, we discuss results associated with a heterogeneous fault with long-range stress-transfer interactions. To better understand earthquake dynamics we focus on faults with Gutenberg-Richter-like earthquake statistics and develop two universal scaling functions as a stronger test of the theory against observations than mere scaling exponents that have large error bars. Universal shape profiles contain crucial information on the underlying dynamics in a variety of systems. As in magnetic systems, we find that our analysis for earthquakes provides a good overall agreement between theory and observations, but with a potential discrepancy in one particular universal scaling function for moment rates. We primarily use mean field theory for the theoretical analysis, since it has been shown to be in the same universality class as the full three-dimensional version of the model (up to logarithmic corrections). The results point to the existence of deep connections between the physics of avalanches in different systems.

I. INTRODUCTION

Earthquake phenomenology is characterized by several power law distributions. The most famous of these are the frequency-size distributions (i.e., histograms) of regional and global earthquakes [1,2], and the modified Omori law for the aftershock decay rate around large rupture zones [3,4]. Using the seismic moment M_0 for the earthquake size, the frequency-size distribution (or moment histogram) has the form (e.g., [5])

$$n(M_0) \sim M_0^{-1-\beta} \qquad (1)$$

where $M_0 \sim \Sigma_i \Delta u_i \Delta A_i$ with Δu_i and ΔA_i being the local slip and rupture area during an earthquake, respectively. A related, more commonly used form in terms of earthquake magnitude M is

$$\ln[n(M)] = a - bM \qquad (2)$$

where $n(M_0)dM_0 = n(M)dM$, the constant a characterizes the overall rate of activity in a region, and the b value gives the relative rates of events in different magnitude ranges. Using the observed moment-magnitude scaling relation $M \sim 2/3 \ln(M_0)$ for large earthquakes [5,6,2], the exponent β of (1) is related to the b value of (2) as $b = 1.5\beta$. The modified Omori law for aftershock decay rates is

$$\Delta N/\Delta t \sim K/(t + c)^p \qquad (3)$$

where N is the cumulative number of aftershocks, t is the time after the mainshock, and K, c, and p are empirical con-

stants. The exponents in (1) and (3) are stable for data collected over large space-time domains, with some clear deviations from global averages related to faulting type and regional properties [2]. For example, the b values of strike-slip, thrust, and normal earthquakes with depth $\leqslant 50$ km in the global Harvard catalog are about 0.75, 0.85, and 1.05, respectively [7]. (Alternatively, Ref. [8] concludes that most of the variability is due to systematic variations in the corner moment required to maintain a finite energy or moment flux.) As another example, regions with high heat flow often have short aftershock sequences with relatively large exponent (e.g., $p > 1.25$), while regions with low heat flow have long aftershock sequences with low exponent (e.g., $p < 0.9$) [3,4]. The association of earthquake statistics with power law relations like Eqs. (1) and (3) led some to suggest that earthquake dynamics is associated with an underlying critical point [9–13]. There are also other independent pieces of evidence that earthquakes are near-critical-point systems [14], e.g., the small and relatively scale-invariant stress drop and the ease with which earthquakes can be triggered by man-made stress perturbations. Power law distributions, however, can be generated by many other mechanisms [15,16] and it is important to develop criteria that can provide stronger evidence for or against the association of earthquakes with criticality.

Recently, enough data have been collected to extract statistics of earthquakes on individual fault zones occupying long (order 100 km) and narrow (order 10 km) regions of space. Wesnousky and collaborators [17,18] found that the frequency-size statistics of earthquakes on highly irregular fault zones, with many offsets and branches, like the San Jacinto fault in California, are also described by the Gutenberg-Richter power law relation up to the largest events. However, relatively regular fault zones (presumably generated progressively with increasing accumulated slip

---

*Electronic address: mehtafree@yahoo.com
†Electronic address: dahmen@uiuc.edu
‡Electronic address: benzion@usc.edu

over time), such as the San Andreas fault in California, display power law frequency-size statistics only for small events. These occur in the time intervals between roughly quasiperiodic earthquakes of a much larger size that is related to large-scale dimensions of the fault zone [5,17–20]. (If the ratio of the mean divided by the standard deviation of the distribution of time intervals between characteristic earthquakes is larger than 1, the distribution is referred to as quasiperiodic [20].) Earthquakes of intermediate magnitude are typically not observed on these faults (other than, perhaps, during aftershock sequences). The corresponding frequency-size statistics are called the "characteristic earthquake" distribution [5,17].

Previously these two types of behavior on individual fault zones have been modeled as statistics close to and far from an underlying critical point [9,21], using a model for a strike-slip fault that incorporates long-range interactions and strong heterogeneities [19,20]. The different dynamic regimes were associated with a competition between failure-promoting effects of elastic stress transfer or dynamic weakening, and the opposing effect of strength inhomogeneities in the fault structure. Fisher *et al.* [9] found that near the critical point the frequency-size statistics follow a power law distribution (with a cutoff at large magnitude), with the same scaling exponent as for observed data for strike-slip faults (i.e., a *b* value of 0.75). A similar form of frequency-size statistics and predicted *b* value were obtained also for a critical parameter value in a stochastic branching model [22].

To provide an improved understanding of earthquake dynamics that can suggest additional observables, we focus on faults with Gutenberg-Richter-like earthquake statistics (i.e., near-critical behavior) and develop two universal scaling *functions* associated with mean moment-rate time profiles at either fixed total moment or fixed total earthquake duration. Universal scaling functions (or shape profiles) give important information on the underlying dynamics, and may be found in solar flares in astrophysics [23], price fluctuations in financial markets [24], Barkhausen noise in magnets [25], and, as shown here, also in earthquake phenomenology. If the behavior of fault zones with earthquakes following the Gutenberg-Richter statistics is indeed critical, then the shapes of these functions should be as universal as the exponent β in Eq. (1). Comparing the scaling functions in our earthquake model to observations constitutes a much stronger test of the theory than merely comparing a discrete, finite set of critical exponents.

In the following we compute the scaling functions for both model predictions and observational data and compare the results. In Sec. II of the paper we review the model. In Secs. III–V, we extend the model, while introducing an extended phase diagram for the model dynamics, and discussing the scaling behavior on long length scales. In Sec. VI we introduce the universal scaling functions and their scaling forms, and in Sec. VII we extract the functions from both simulation and observational data. Finally, in Sec. VIII we discuss the results and emerging new questions.

II. EARTHQUAKE MODEL

The model we use was developed originally by Ben-Zion and Rice [19,20], who suggested that a narrow irregular
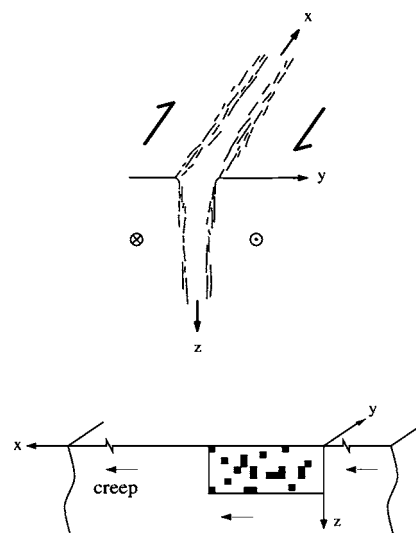

FIG. 1. A planar representation of a 3D segmented fault zone by a 2D heterogeneous fault embedded in a 3D solid [19,20].

strike-slip fault zone of horizontal length L and vertical depth W may be represented by an array of $N \sim LW$ cells in a two-dimensional plane, with constitutive parameters that vary from cell to cell to model the disorder (offsets, etc.) of the fault zone structure (Fig. 1). The cells represent brittle patches on the interface between two tectonic blocks that move with slow transverse velocity v in the x direction at a great distance from the fault. The interaction between cells during slip events is governed by three-dimensional (3D) elasticity and falls off with the distance r from the failure zone as $1/r^3$. These interactions are sufficiently long range that scaling in mean field theory (where the interaction range is set to infinity) becomes exact, up to logarithmic corrections, in the physical fault dimension ($d=2$) [9,19,20].

In mean field theory, the local stress τ_i on a given cell i is [19]

$$\tau_i = (J/N)\sum_j (u_j - u_i) + K_L(vt - u_i) \qquad (4)$$

$$= J\bar{u} + K_L vt - (K_L + J)u_i \qquad (5)$$

where u_i is the total offset of the cell in the horizontal x direction, $\bar{u} = \sum_j u_j/N$ is the average displacement, J/N is the mean field elastic coupling strength between cells, and $K_L \sim 1/\sqrt{N}$ is the loading stiffness [21] of the tectonic blocks that move far away from the fault with relative velocity v. Initially the stresses τ_i are randomly distributed with $\tau_{a,i} \leq \tau_i \leq \tau_{s,i}$, where $\tau_{s,i}$ is a fixed local *static* failure threshold stress and $\tau_{a,i}$ is the fixed local arrest stress. The distributions of static failure stresses and arrest stresses represent the heterogeneity or geometrical disorder in the fault system. The differences between the failure and arrest stresses give the local distribution of stress drops during brittle failures; the earthquake dynamics depend only on the stress drop distribution (no other quenched randomness). In addition, the scaling behavior of the system is not sensitive to the exact form of the distributions as long as they are bounded and
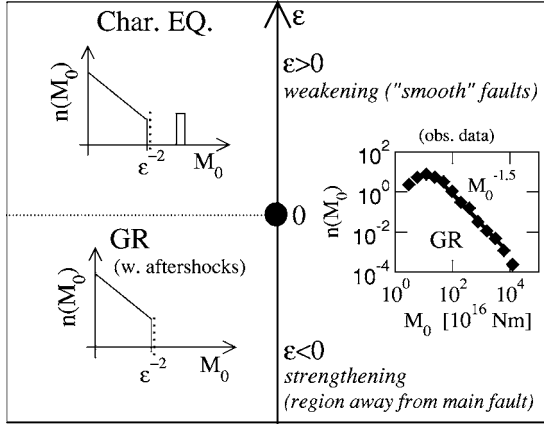
FIG. 2. Phase diagram of the model (see text and [21] for details).

$\tau_{a,i} < \tau_{s,i}$. We choose a compact distribution for $\tau_{a,i}$, such that $p(\tau_{a,i}) = 3(W^2 - 4\tau_{a,i}^2)/(2W^3)$ for $-W/2 \leq \tau_{a,i} \leq W/2$ and 0 outside of these bounds. Also, we look at the low-disorder limit where $W \ll \tau_{s,i}$, where we choose $\tau_{s,i} = 1$, so all cells will fail at this point.

The fault is stuck while the stress on each cell is increased uniformly as $d\tau_i/dt = K_L v$ as a result of the external loading which is increased adiabatically (that is, we take the limit $v \to 0$). When the stress on a cell reaches its failure threshold $\tau_{s,i}$, the cell slips by the amount

$$\Delta u_i = (\tau_{s,i} - \tau_{a,i})/(K_L + J). \tag{6}$$

This stress drop is uniformly redistributed to all other cells (employed in the mean field approximation) by an amount

$$\delta\tau_j = (c/N)(\tau_{s,i} - \tau_{a,i}), \quad j \neq i, \tag{7}$$

where $c \equiv J/(K_L + J)$ is the conservation parameter which gives the fraction of the stress drop of a cell that is retained in the system after it slips [21]. The resulting stress increase on the other cells can cause some of them to slip as well, leading to an avalanche of cell slips, or an earthquake.

III. DYNAMICAL WEAKENING AND STRENGTHENING

The model includes dynamic weakening effects during the failure process [19,20]: after an initial slip in an earthquake, the strength of a failed cell is reduced to a *dynamical* value

$$\tau_{d,i} \equiv \tau_{s,i} - \epsilon(\tau_{s,i} - \tau_{a,i}), \tag{8}$$

with $0 \leq \epsilon \leq 1$ parametrizing the relative importance of dynamical weakening effects in the system. This weakening represents the transition from static friction to dynamic friction during the rupture and the strength of a failed cell remains at the dynamic value throughout the remainder of the earthquake. In the time intervals between earthquakes all failure thresholds heal back to their static value $\tau_{s,i}$. Fisher *et al.* [9] found that at exactly $\epsilon = 0$ the model produces a power law distribution of earthquake moments M_0 following Eq. (1), cutoff by the finite fault size, with an analytical exponent $\beta = 1/2$ (Fig. 2). This corresponds to a b value of 0.75, close

to that associated with observed earthquakes on strike-slip faults [7]. The power law scaling of the frequency-size statistics and other variables [9] indicates that the model with $\epsilon = 0$ operates at a critical point. In contrast, for a finite weakening $\epsilon > 0$ the model produces the characteristic earthquake distribution, with power law statistics for the small events up to a cutoff moment that scales as

$$M_0^{cutoff} \sim 1/\epsilon^2, \tag{9}$$

and quasiperiodically recurring large characteristic events that scale with the fault size $[M_0 \sim (LW)^{3/2}]$.

The model can be expanded further to include dynamic strengthening represented by $\epsilon < 0$. Ben-Zion and Sammis [26] summarized multidisciplinary observations which indicate that brittle failure of rock has an initial transient phase associated with strengthening, distributed deformation, and creation of new structures. Detailed frictional studies also show an initial strengthening phase associated with the creation of a new population of asperity contacts [5,27]. In our model (Fig. 1) we associate $\epsilon < 0$ with regions off the main fault segments that are in an early deformation stage. To capture basic aspects of brittle deformation on such regions in the three-dimensional volume around the main fault (Fig. 1), we change the model as follows. When any cell i slips during an earthquake, and thereby reduces its stress by $\Delta\tau_i \equiv \tau_{f,i} - \tau_{a,i}$, the failure stress $\tau_{f,j}$ of *every* cell $j = 1, \ldots, N$ is *strengthened* by an amount $|\epsilon|\Delta\tau_i/N$. Once the earthquake is complete, the failure stress of each cell is slowly lowered back to its original value. This represents in a simple way the brittle deformation that occurs during an earthquake in the off-fault regions, which are first in a strengthening regime, compared to the main fault, and then have a weakening process. The events that are triggered as the failure stresses are lowered in the weakening period are referred to as *aftershocks*. The occurrence of aftershocks in this version of the model for off-fault regions is in agreement with the observation that a large fraction of observed aftershocks typically occur in off-fault regions [28]. For this version of the model with $\epsilon < 0$, both the primary earthquakes (i.e., main shocks) and the triggered aftershocks are distributed according to the Gutenberg-Richter distribution, up to a cutoff moment scaling as $1/\epsilon^2$. Assuming that the increased failure stress thresholds $\tau_{f,i}$ are slowly lowered with time as $\ln(t)$ toward their earlier static values $\tau_{s,i}$, and that the stresses are distributed over a wide range of values, we show analytically in the Appendix that the temporal decay of aftershock rates at long times is proportional to $1/t$, as in the modified Omori law of Eq. (3) with $p = 1$ [3–5].

Remarkably, the long-length-scale behavior of this model can be shown [29,30] to be the same as the behavior of the model given in Eq. (5) with an added "antiferroelastic" term $(-|\epsilon|J\bar{u})$:

$$\tau_i = J\bar{u} + K_L vt - (K_L + J)u_i - |\epsilon|J\bar{u}. \tag{10}$$

In Eq. (10) every time a cell fails, it slips by an amount Δu_i which leads to stress loading of the other cells, lessened by $|\epsilon|J\Delta u_i/N$ compared to our original model [Eq. (5)]. On the other hand, in the global strengthening model (described

above) when a cell slips the failure stresses of all cells are strengthened by $|\epsilon|J\Delta u_i/N$. On long length scales the global strengthening of the failure stress has equivalent effects on the earthquake statistics as the dissipation of the redistributed stress, up to corrections of order $O(1/N)$, so the scaling behavior for large events of both models is the same. Moreover, Eq. (10) can be rewritten as

$$\tau_i = J[1 - |\epsilon|][\bar{u} - u_i] + K_L vt - [K_L + J|\epsilon|]u_i. \quad (11)$$

We can now absorb $|\epsilon|$ by defining $J' = J(1 - |\epsilon|)$ and $K_L' = K_L + J|\epsilon|$. Rewriting Eq. (11) with the new definitions, and dropping the $|\epsilon|$ contribution in $[K_L' - J|\epsilon|]vt$ since $v \to 0$, we find

$$\tau_i = J'\bar{u} + K_L'vt - (K_L' + J')u_i. \quad (12)$$

Therefore we recover Eq. (5) with $J \to J'$ and $K_L \to K_L'$. This amounts to changing the stress conservation parameter c (from Ref. [21]). For Eq. (12)

$$c = J'/(K_L' + J') = 1 - |\epsilon| \quad (13)$$

where $K_L \to 0$ since we are concerned with the adiabatic limit. We also know (from Ref. [21]) that the cutoff S_{cf} for the Gutenberg-Richter distribution scales as $S_{cf} \sim 1/(1-c)^2$. Thus, from Eq. (13) we find that the cutoff for Eq. (10) will scale as $\sim 1/|\epsilon|^2$.

IV. MAPPING TO SINGLE-INTERFACE MAGNET MODEL

The mean field version of the single-interface magnet model with infinite-range antiferromagnetic interactions is given by [31,32]

$$\dot{h}_i(t) = J[\bar{h} - h_i(t)] + H(t) - k\bar{h} + \eta_i(h) \quad (14)$$

where $h_i(t)$ is the position of the domain wall, $H(t)$ is the external driving field, k is the coefficient of the antiferromagnetic term, and $\eta_i(h)$ is the pinning field. In the paper by Fisher *et al.* [9] it has been shown that the scaling behavior on long length scales resulting from Eq. (10), without the $-|\epsilon|J\bar{u}$ term, is the same as that of Eq. (14) without the antiferromagnetic term $-k\bar{h}$. Furthermore, upon inspection we see the following correspondence between the single-interface magnet model [Eq. (14)] and the mean field earthquake model [Eq. (10)]:

$$-k\bar{h} \Leftrightarrow -|\epsilon|J\bar{u}. \quad (15)$$

In other words, the coefficient of the antiferromagnetic term k plays the same role in the magnet model [Eq. (14)] as the coefficient of strengthening $|\epsilon|J$ does in the earthquake model [Eq. (10)].

V. PHASE DIAGRAM

The regimes with various statistics produced by the model are summarized by the phase diagram given in Fig. 2. The range $\epsilon > 0$ corresponds to "mature" localized faults with a weakening rheology and characteristic earthquake statistics. The value $\epsilon = 0$ corresponds to "immature" strongly inhomo-

geneous fault zones with Gutenberg-Richter statistics. Finally, the range $\epsilon < 0$ corresponds to the fracture network away from the main fault, characterized by strengthening due to the creation of new structures and associated emerging aftershocks. It may be surprising that the discussed simple model can capture many of the essential general features of earthquake statistics (or other systems with avalanches, such as driven magnetic domain walls). This can be understood through the renormalization group [34,33], a powerful mathematical tool to coarse-grain a system and extract its effective behavior on long space-time scales. Many microscopic details of a system are averaged out under coarse graining, and universal aspects of the behavior on long scales depend only on a few basic properties such as symmetries, dimensions, range of interactions, weakening or strengthening, etc. When a model correctly captures those basic features, the results provide proper predictions for statistics, critical exponents, and universal scaling functions near the critical point. Consequently, many models that are in the same universality class lead to the same statistics and exponents [9,21,33,34]. The universal scaling functions around the critical point, discussed in the next section, provide additional information that can be used to distinguish between different models and universality classes.

VI. MOMENT RATE SHAPES

In this section we focus on fault zones with Gutenberg-Richter power law statistics, modeled by systems at or close to the $\epsilon = 0$ critical point. Recent analysis allowed researchers to obtain the moment rate $dm_0(t)/dt$, which gives the slip on a fault per unit time during the propagation of earthquake rupture, for hundreds of large seismic events recorded on global networks [35,36]. The moment rates are derived from inversions of teleseismically recorded seismograms on a global seismic network [37]. Motivated by works on statistical physics of magnetic systems discussed in the previous chapter (see also [25,34]), we are interested in studying the event-averaged moment rate time profile (Fig. 3) for earthquakes with given total moment M_0, denoted by $\langle dm_0(t|M_0)/dt \rangle$ and the event-averaged moment rate time profile (Fig. 4) for earthquakes with given duration T, denoted by $\langle dm_0(t|T)/dt \rangle$. Here $m_0(t|T)$ is the (cumulative) moment at time t of the propagating earthquake of total duration T, and $m_0(t|M_0)$ is the cumulative moment at time t of the earthquake of total moment M_0. Theoretical analysis of phase diagrams similar to that shown in Fig. 2 implies that near the critical point there should be, in addition to scaling exponents, also universal scaling functions (up to a rescaling of the ordinate and abscissa) [25]. In our model both in mean field theory and in simulations, the two scalable functions of interest, $\langle dm_0(t|M_0)/dt \rangle$ and $\langle dm_0(t|T)/dt \rangle$, obey, respectively, the following scaling relations [9,25,29,38] (up to negligible logarithmic corrections):

$$\langle dm_0(t|M_0)/dt \rangle/M_0^{1/2} \sim f(t/M_0^{1/2}) \quad (16)$$

and
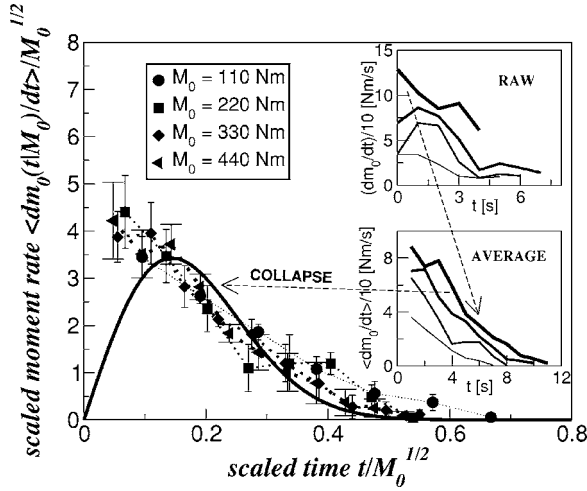
$$\langle dm_0(t|T)/dt \rangle \sim g(t/T). \quad (17)$$

FIG. 3. A collapse of averaged earthquake pulse shapes, $\langle dm_0(t|M_0)/dt \rangle$, with the size of the moment M_0 in N m within 10% of each size given in the legend. In order to obtain each collapsed moment rate shape, five to ten earthquakes were averaged for each value of M_0. The collapse was obtained using the mean field scaling relation [9]: $\langle dm_0(t|M_0)/dt \rangle / M_0^{1/2} \sim f(t/M_0^{1/2})$ [see text Eq. (16)]. In our mean field theory the universal scaling function is $f_{mf}(x) = Axe^{-Bx^2/2}$ where $x = t/M_0^{1/2}$. We plot this functional form (bold curve) with $A=4$ and $B=4.9$. Inset: The raw data and the averaged data (before collapse).

We determined these scaling functions from corresponding mean field results for magnets, using the fact that both the mean field version of the Ben-Zion and Rice model of Eq. (5) [9,21] and the simulation with the full 3D stress transfer along the fault (up to logarithmic corrections) are in the same universality class (i.e., have the same universal be-
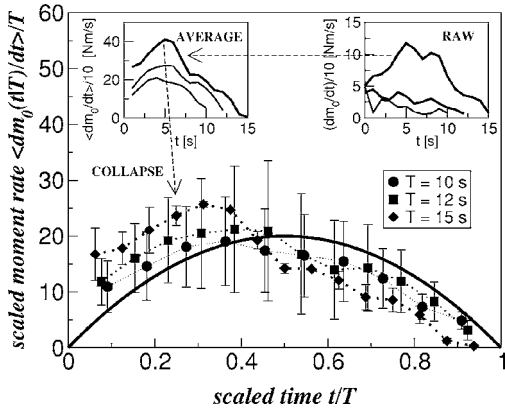

FIG. 4. A collapse of averaged earthquake pulse shapes, $\langle dm_0(t|T)/dt \rangle$ with a duration of T (seconds) within 10% (given in legend), is shown. The collapse was obtained using the mean field scaling relation [38]: $\langle dm_0(t|T)/dt \rangle \sim g(t/T)$. In order to obtain each collapsed pulse shape, two to ten earthquakes were averaged for each value of T. In our mean field theory the universal scaling function is $g_{mf}(x) = Ax(1-x)$ with $x = t/T$. We plot this functional form (bold curve) with $A=80$. Note the apparent asymmetry to the left in the observed data while the theoretical curve is symmetric around its maximum. Inset: The raw data and the averaged data (before collapse).

havior on long length scales) as the above mentioned mean field model for domain wall motion in magnets.

VII. EXPONENTS AND DATA COLLAPSES

We compare the observation results with our model and find remarkable agreement in most cases. The frequency-moment distribution $D(M_0) \sim M_0^{1-\beta}$ of the observed data [35] has (inset of Fig. 2) three decades of scaling and an exponent of $\beta = 1/2 \pm 0.05$, in close agreement with the model near $\epsilon = 0$. The deviation from a power law distribution at the low-moment range is associated with the reduced resolution of the observational network for small events. In mean field theory the universal scaling function $f(x)$ in Eq. (16) is of the exact form [39] $f_{mf}(x) = Axe^{-Bx^2/2}$ with nonuniversal constants $A = B = 1$. In Fig. 3 we present a collapse of the observational data of $\langle dm_0(t|M_0)/dt \rangle$ for four different values of M_0 to obtain the corresponding function $f_{exp}(x)$ for observations with $x = t/M_0^{1/2}$. The observational curves not only collapse, and are therefore *universal*, the mean field exponent $1/2$ in the scaling variable x is in excellent agreement with observations. We fit the functional form $f_{mf}(x)$ with $A=4$ and $B=4.9$ to the collapse of the observed data; $f_{exp}(x)$ deviates from $f_{mf}(x)$ for small values of the ordinate.

In mean field theory, the function $g(x)$ of Eq. (17) is of the symmetric form $g_{mf}(x) = Ax(1-x)$, where A is a nonuniversal constant. In Fig. 4 we collapse observational data for $\langle dm_0(t|T)/dt \rangle$ for three values of T to obtain the function $g_{exp}(x)$ with $x = t/T$. Again we find that the curve collapses well, even though only small data sets were available, and the exponent of 1 obtained from the collapse is in excellent agreement with mean field theory.

We also plot the mean field scaling function $g_{mf}(x)$ with $A=80$. The results show that while the scaling exponents agree, there are notable differences between the observational function $g_{exp}(x)$ and the mean field function $g_{mf}(x)$, especially for small values of the ordinate. We checked that finite-size effects do not play a role in $g_{mf}(x)$ [or in $f_{mf}(x)$ for that matter]. Also, we find that the mean skewness coefficient for the $g_{exp}(x)$ curves is 0.878 and the mean standard error of skewness is 0.705: since twice the standard error is greater than the absolute value of the skewness, the asymmetry is not statistically significant. Therefore more observational work with a larger data set is required to verify the moment rate shape asymmetry and clarify its origin. An asymmetry may result from a rupture process that begins with a failure of a large asperity, from finite fault size effects if the rupture process slows down once the rupture has traversed the fault in one direction, or from contributions of early aftershocks.

VIII. DISCUSSION

The employed earthquake model [19,20] was shown in the past to have a critical point at $\epsilon = 0$ and additional dynamic regimes for $\epsilon > 0$ [9,21] compatible with observed frequency-size statistics of earthquakes on individual fault zones [17,18]. We have generalized the theoretical analysis to include a strengthening regime $\epsilon < 0$ with aftershocks, and

derived universal scaling functions around the critical point $\epsilon=0$. The results provide new tools for data analysis that may be used to obtain an improved understanding of earthquake dynamics. The analysis indicates that near $\epsilon=0$ the model is in the same universality class as a recent model for domain wall motion in magnets and we can match the phase diagram regions $\epsilon<0$ and $\epsilon>0$ to those of the corresponding magnet model [9,32,34,38]. In other words, the two systems are marked by the exact same universal scaling exponents, universal scaling functions, and similar phase diagrams. The model predictions for frequency-size statistics and moment rates of earthquakes near $\epsilon=0$ are overall in close agreement with observational data of relatively large earthquakes recorded on the global seismic network [35]. However, the observed mean moment rate of earthquakes with a given duration T apparently increases with time more rapidly than it drops off, contrary to the corresponding symmetric model function. The potential asymmetry in the observed data may result from a rupture process that begins with a failure of a large asperity. This is compatible with observations that hypocenter locations tend to be located close to an area on a fault that produces large moment release (e.g., [40]). As we explain below, an analogy to magnetic systems suggests that an asymmetry could potentially also stem from momentary initial threshold strengthening associated with the creation of a new population of asperity contacts upon local failure [27] and followup aftershocks. Further study will be necessary to clarify this issue.

Theoretical analysis of such a potential asymmetric rupture process requires corrections to the mean field earthquake model results. Recently it has been shown that the corresponding magnetic domain wall model [25,34] predicts well the critical scaling exponents for Barkhausen noise experiments in magnets. Significantly, the experimental scaling function for magnetization avalanches or Barkhausen "pulses" [25,34], that is the analog of the moment rate time profile for fixed earthquake duration of Eq. (17), shows the same type of asymmetry that is apparently observed for earthquakes (Fig. 4). It has been suggested that the asymmetry in the function is due to eddy currents in the magnet [41,42]. Eddy currents have a similar effect in magnets as transient threshold strengthening would have on earthquakes. In this paper we have shown how long-term threshold strengthening (on time scales longer than individual earthquakes) leads to aftershocks, which effectively represent an asymmetry on time scales longer than individual earthquakes. This raises the possibility that the origin of this asymmetry may be similar in both magnets and earthquakes [42]: in both cases it may be due to a transient force (due to eddy currents or threshold strengthening respectively) that counteracts the propagation of an event and thus leads to asymmetric event profiles that taper off more slowly than they began. Our study shows that there are important theoretical and observational connections between processes in earthquake and magnetic systems.

A related study of earthquake moment rate shapes was done by Houston [43] who used a data set similar to the data of Bilek [35] used here. In order to compare the average moment rate profiles of these earthquakes, the profiles were rescaled by two methods: moment scaling and duration scal-
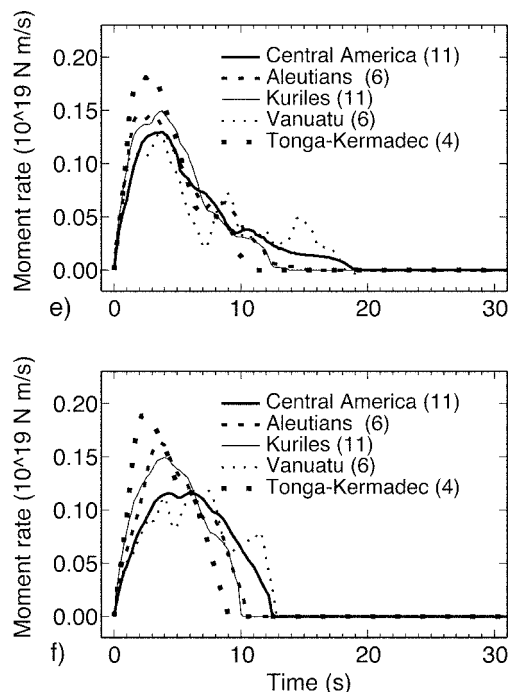

FIG. 5. Rescaled moment rate versus time profiles of seismic events determined with moment scaling (top) and duration scaling (bottom) by [43] (see text). The data shown are obtained from several subduction zones in the indicated geographical locations and the numbers of earthquakes used for each region are given in parentheses.

ing. Moment scaling rescales the time axis of the profiles using assumptions about cracklike scaling of the events (different from our mean field result), and then rescales the height of the profiles so that the area (or moment) under all profiles is the same. The duration scaling of [43] rescales the time axis such that all duration-scaled profiles end at the same reference duration, and then rescales the moment rates so that all scaled time profiles have the same area underneath.

Figure 5 shows average moment rate profiles that were obtained by Houston from moment scaling (top) and duration scaling (bottom) for data from several subduction zones. The top plots correspond to $\langle dm_0(t|M_0)/dt \rangle$ collapsed, and the bottom plots correspond to $\langle dm_0(t|T)/dt \rangle$ collapsed. We see from the top part in Fig. 5 that overall the moment rate shapes seem to agree rather well with our predicted mean field shapes of Fig. 3. Likewise the bottom plots of Fig. 5 appear to agree quite well with the mean field curve of Fig. 4, except for an additional slight asymmetry, with positive skewness, similar to our result from observations.

In [43] the skewness of the duration scaled moment rate profiles, i.e., the skewness of the $\langle dm_0(t|T)/dt \rangle$ collapses, is calculated and found to range from 0.12 to 0.36 depending on the depth of the earthquakes (bigger skewness for greater depth) and the method used to extract moment rates from seismograms. Since the statistical error of the skewness is not given in [43], we cannot determine if the above skewness values are statistically significant. It is interesting, however, that just as in the case of magnets, and in our analysis of the

observational data, the skewness is slightly positive, indicating that on average earthquakes tend to grow faster than they die down. The skewness values quoted in [43] are smaller than the 0.878 value obtained here, though one of them (the 0.36 value for earthquakes at greater depth) is within error bars.

While overall the shapes of the moment rate profiles look rather similar for both Houston's analysis and our mean field theory results, there are significant differences in the analysis that can be summarized as follows.

(1) The exponents used in [43] to create the moment-scaled average profile $\langle dm_0(t|M_0)/dt \rangle$ differ from the exponents we used. In both cases the x axis is divided by $M_0^{\alpha_t}$ and the y axis is divided by $M_0^{1-\alpha_t}$ in order to ensure normalization of the curves to a fixed reference moment. In [43] the exponent value is $\alpha_t = 1/3$, while in this paper we use the mean field value $\alpha_t = 1/2$ (see Fig. 3). The value $\alpha_t = 1/3$ in [43] is associated with cracklike scaling; for cracks the moment M_0 scales with the rupture area A as $M_0 \sim A^{3/2}$ [5]. Since the rupture area scales with the diameter L of the crack as $A \sim L^2$ and the duration T of the earthquake scales with its diameter as $T \sim L$ one arrives at the proposed scaling $T \sim M_0^{1/3}$. In [43] it is mentioned, however, that the data would also be compatible with rescaling the time (or x) axis with an exponent of $\alpha_t \simeq 0.41$, i.e., that $T \sim M_0^{0.41}$ for the data. This scaling is much closer to the mean field prediction $T \sim M_0^{1/2}$, i.e., $\alpha_t = 1/2$, that is used in this work.

Our exponent $\alpha_t = 1/2$ is derived from the mean field prediction [9] that the duration T of earthquakes in the critical power law region of Fig. 2 scales as $T \sim M_0^{1/2}$. In [9] it is shown analytically that the moment M_0 of earthquakes in the critical regime scales with the rupture area as $M_0 \sim A$. Since the rupture area scales, as before, with the earthquake diameter as $A \sim L^2$, and the earthquake duration scales as $T \sim L$, one obtains for the mean field prediction $T \sim M_0^{1/2}$ for critical earthquakes. Note that for earthquakes which are so large that their horizontal diameter L is much larger than the vertical width of the fault, one expects the moment to scale as $M_0 \sim L$. Since again the duration scales as $T \sim L$, one obtains $T \sim M_0$, i.e., $\alpha_t = 1$. The data used here and in [43] apparently do not fall within this scaling regime.

(2) Our theoretical analysis leads to predictions of both scaling exponents and entire scaling functions, which can be compared to data. In contrast, in [43] the shape is obtained only empirically by averaging rescaled data, and it is dependent on the chosen scaling exponents. Our procedure of comparing the theoretical results to data is designed to provide simultaneously, through a scaling collapse that minimizes deviations of individual averaged curves from the collapsed one, the scaling exponent α_t and the entire scaling function. On the other hand, in [43] the value of α_t is obtained from a separate analysis of duration versus moment of observed data, and the shape is then obtained empirically, by averaging rescaled data.

(3) For our simulated moment rates, the exponents used in [43] would not lead to a good collapse, i.e., the deviation between various rescaled curves would be larger for $\alpha_t = 1/3$ compared to $\alpha_t = 1/2$.

Unfortunately, since the available observational data have large error bars, we cannot determine at present unequivocally, which set of exponents works better. More moment rate data, especially for many small earthquakes would allow us to reduce statistical error bars and obtain a more precise comparison of the scaling functions in theory and experiment. The smaller earthquakes are also more likely to fall into the critical scaling regime of our mean field prediction. However, moment rate data are more difficult to obtain for small earthquakes, as they require greater spatial resolution. We hope that this study will motivate more observational work and analysis to answer these questions.

ACKNOWLEDGMENTS

APPENDIX: DETERMINATION OF OMORI LAW OF AFTERSHOCK DECAY

We derive the Omori law for aftershock decay from our mean field earthquake model in the case of dynamic strengthening. After a primary earthquake, the static failure stress τ_s is increased by an amount $\epsilon\langle s \rangle/N$, where $\langle s \rangle$ is the mean event size. Given in terms of moment, the mean avalanche size in mean field theory is simply given by [21]

$$\langle s \rangle = \int_0^{1/\epsilon^2} s/s^{3/2} ds \sim 1/\epsilon \qquad (A1)$$

where $1/s^{3/2} \sim D(s)$, is the scaling behavior of the mean field event size distribution. Now since $\langle s \rangle \sim 1/\epsilon$, the failure stress τ_s is then shifted by an amount $1/N$.

In order to produce aftershocks, we assume that the new larger failure stress, which we call τ_f^0, is lowered slowly, logarithmically in time, until it returns to its original value $\tau_s \simeq \tau_f^0 - 1/N$. More precisely, using $t=0$ for the time at the end of the previous earthquake, τ_f^0 decays as follows:

$$\tau_f(t) = \tau_f^0[1 - \ln(1 + t)]. \qquad (A2)$$

We define $\eta(t)$ as the amount by which τ_f^0 has been lowered at time t:

$$\eta(t) = \tau_f^0 - \tau_f(t) = \tau_f^0 \ln(1 + t). \qquad (A3)$$

Equation (A2) is only accurate to first order since lowering the threshold triggers on average $\sim \eta(t)$ aftershocks (assuming nonsingular stress distributions). Since aftershocks occur

quickly compared to the weakening time scale, the aftershocks that are triggered due to lowering the threshold will cause $\tau_f(t)$ to shift up by: $\eta(t) \times \epsilon \langle s \rangle / N \sim \eta(t)/N$. Thus the expression for $\tau_f(t)$ becomes

$$\tau_f(t) = \tau_f^0[1 - \ln(1+t)] + \eta(t)/N \qquad (A4)$$

and Eq. (A3) gives

$$\eta(t) = \tau_f^0 \ln(1+t) - \eta(t)/N, \qquad (A5)$$

$$\eta(t) = \frac{\tau_f^0 \ln(1+t)}{1 + 1/N}. \qquad (A6)$$

If we assume that the number of aftershocks triggered by time t is $A(t) \sim \eta(t)$, we obtain the modified Omori law [Eq. (3)] for aftershock decay [3–5]:

$$\frac{\partial A(t)}{\partial t} \sim \frac{\tau_f^0}{(1+t)(1+1/N)}. \qquad (A7)$$

For large t and large N we have the original Omori law:

$$\frac{\partial A(t)}{\partial t} \sim \frac{\tau_f^0}{t}. \qquad (A8)$$

[1] B. Gutenberg and C. F. Richter, *Seismicity of Earth and Associated Phenomena* (Princeton University Press, Princeton, NJ, 1954).

[2] T. Utsu, in *International Handbook of Earthquake and Engineering Seismology*, edited by W. H. K. Lee, H. Kanamori, P. C. Jennings, and C. Kisslinger (Academic, New York, 2002), Part A, pp. 719–732.

[3] Y. Utsu, Y. Ogata, and R. S. Matsu'uara, J. Phys. Earth **43**, 1 (1995).

[4] C. Kisslinger and L. M. Jones, J. Geophys. Res. **96**, 947 (1991).

[5] Y. Ben-Zion, in *International Handbook of Earthquake and Engineering Seismology*, (Ref. [2]), Part B, Appendix 2, pp. 1857–1875.

[6] T. C. Hanks and H. Kanamori, J. Geophys. Res. **84**, 2348 (1979).

[7] C. Frohlich and S. D. Davis, J. Geophys. Res. **98**, 631 (1993).

[8] Y. Kagan, Geophys. J. Int. **148**, 520 (2002).

[9] D. S. Fisher, K. Dahmen, S. Ramanathan, and Y. Ben-Zion, Phys. Rev. Lett. **78**, 4885 (1997).

[10] S. Zapperi, P. Ray, H. E. Stanley, and A. Vespignani, Phys. Rev. E **59**, 5049 (1999).

[11] P. Bak, C. Tang, and K. Wiesenfeld, Phys. Rev. A **38**, 364 (1988).

[12] D. Sornette and C. G. Sammis, J. Phys. I **5**, 607–619 (1995).

[13] W. Klein, M. Anghel, C. D. Ferguson, J. B. Rundle, and J. S. Sà Martins, *GeoComplexity and the Physics of Earthquakes*, Geophysics Monograph Series Vol. 120, edited by J. B. Rundle, D. L. Turcotte, and W. Klein (American Geophysical Union, Washington, DC., 2000), pp. 43–71.

[14] I. Main, Rev. Geophys. **34**, 433 (1996).

[15] M. Schroeder, *Fractals, Chaos, Power Laws* (W. H. Freeman and Co., San Francisco. 1991).

[16] D. Sornette, *Critical Phenomena in Natural Sciences, Chaos, Fractals, Self-Organization, and Disorder: Concepts and Tools* (Springer-Verlag, Berlin, 2000).

[17] S. G. Wesnousky, Bull. Seismol. Soc. Am. **84**, 1940 (1994).

[18] M. W. Stirling, S. G. Wesnousky, and K. Shimazaki, Geophys. J. Int. **124**, 833 (1996).

[19] Y. Ben-Zion and J. R. Rice, J. Geophys. Res. **98**, 14109 (1993).

[20] Y. Ben-Zion, J. Geophys. Res. **101**, 5677 (1996); Y. Ben-Zion and J. R. Rice, *ibid.* **100**, 12959 (1995).

[21] K. Dahmen, D. Ertas, and Y. Ben-Zion, Phys. Rev. E **58**, 1494 (1998).

[22] D. Vere-Jones, Pure Appl. Geophys. **114**, 711 (1976).

[23] E. T. Lu, R. J. Hamilton, J. M. McTiernan, and K. R. Bromond, Astrophys. J. **412**, 841 (1993).

[24] J. P. Bouchaud and M. Potters, *Theory of Financial Risks: From Statistical Physics to Risk Management* (Cambridge University Press, Cambridge, U.K., 2000).

[25] A. P. Mehta, A. C. Mills, K. Dahmen, and J. P. Sethna, Phys. Rev. E **65**, 046139 (2002).

[26] Y. Ben-Zion and C. G. Sammis, Pure Appl. Geophys. **160**, 677 (2003).

[27] J. H. Dieterich, J. Geophys. Res. **84**, 2161 (1979); , Amer. Geophys. Union Monog. **24**, 103 (1981).

[28] J. Liu, K. Sieh, and E. Hauksson, Bull. Seismol. Soc. Am. **93**, 1333 (2003).

[29] A. P. Mehta, Ph.D. thesis, University of Illinois at Urbana Champaign, 2006 (unpublished).

[30] Karin A. Dahmen and Y. Ben-Zion (unpublished).

[31] S. Zapperi, P. Cizeau, G. Durin, and H. E. Stanley, Phys. Rev. B **58**, 6353 (1998).

[32] G. Durin and S. Zapperi, J. Magn. Magn. Mater. **242–245**, 1085 (2002).

[33] J. J. Binney, N. J. Dowrick, A. J. Fisher, and M. E. J. Newman, *The Theory of Critical Phenomena* (Oxford University Press, Oxford, 1993).

[34] J. P. Sethna, K. A. Dahmen, and C. R. Myers, Nature (London) **410**, 242 (2001).

[35] S. L. Bilek, Ph.D. thesis, University of California, Santa Cruz, 2001 (unpublished).

[36] Y. Tanoika and L. Ruff, Seismol. Res. Lett. **68**, 386 (1997).

[37] L. J. Ruff and A. D. Miller, Pure Appl. Geophys. **142**, 101 (1994).

[38] M. C. Kuntz and J. P. Sethna, Phys. Rev. B **62**, 11699 (2000).

[39] D. S. Fisher, Phys. Rep. **301**, 113 (1998).

[40] P. M. Mai, P. Spudich, and J. Boatwright, Seismol. Res. Lett. **74**, 208 (2003); P. M. Mai, P. Spudich, and J. Boatwright, Bull. Seismol. Soc. Am. **95**, 965 (2005).

[41] G. Durin (unpublished).

[42] S. Zapperi, C. Castellano, F. Colaiori, and G. Durin, Nat. Phys. **1**, 46–49 (2005); K. Dahmen, *ibid.* **1**, 13 (2005).

[43] H. Houston, J. Geophys. Res. **106**, 11137 (2001).